RSC Advances

ROYAL SOCIETY OF CHEMISTRY

www.rsc.org/advances

Effect on physical and chemical characteristics of activated carbon on adsorption of trimethoprim: Mechanisms study

Hai Liu[a,d], *Jian Zhang*[*,a], *Huu Hao Ngo*[b], *Wenshan Guo*[b], *Haiming Wu*[c], *Zizhang Guo*[a], *Cheng Cheng*[a], *Chenglu Zhang*[a]

[a]*Shandong Key Laboratory of Water Pollution Control and Resource Reuse, School of Environmental Science and Engineering, Shandong University, Jinan 250100, China*

[b]*School of Civil and Environmental Engineering, University of Technology Sydney, Broadway, NSW 2007, Australia*

[c]*College of Resources and Environment, Northwest A & F University, Yangling, Shaanxi 712100, China*

[d]*Department of Chemical and Biomolecular Engineering, University of California, Berkeley, California 94720, United States*

Abstract

Five different types of activated carbon varying in porosity, structures, and functional groups, were prepared and used as adsorbents. The effect of key properties of each activated carbon on its adsorption capacity, rate and mechanisms in terms of trimethoprim (TMP) removal were evaluated. The kinetics results suggested that chemical adsorption interactions and particle diffusion into micropores were the main rate-control steps for TMP adsorption, and the existence of mesopores promoted the diffusion of TMP into internal pores. The adsorption of TMP onto activated carbon could be attributed to the pore-filling effect (micropores and some narrow mesopores) and strong adsorptive interactions with the graphene surface or oxygenated groups. Regarding the surface area-normalized adsorption of TMP, porous activated carbon exhibited 50-500 times lower than nonporous carbon adsorbent due to the

*** Corresponding author:** Tel.: + 86 531 88363015; Fax: +86 531 88364513; E-mail address: zhangjian00@sdu.edu.cn (J. Zhang); shandaliuhai@ berkeley.edu (H. Liu).

size-exclusion effect, especially when oxygen complexes representing on the edges of pores of activated carbon. As from a system design point of view, fast adsorption rate and high adsorption capacity are normally required, the findings implied that activated carbon with high microporosity, certain mesoporosity and approachable surface groups can have a great application potential for TMP removal.

Keywords: Activated carbon; Adsorption; Trimethoprim; Mechanism

1. INTRODUCTION

As a highly effective dihydropteroate synthetase inhibitor, trimethoprim (TMP) has been prescribed for more than 60 years to treat various bacterial infections both for human and veterinary use. Hence, it is regarded as one of the most essential medicines for basic health system by the World Health Organization [1, 2] and particularly recommended for treating tuberculosis [3] and reducing opportunistic infections for adults with HIV/AIDS [4]. Due to its high effectiveness and low cost (approximate 16-32 USD/Kg) [5], a large quantity of TMP has been produced and prescribed, for instance, as reported by Chinese Medical Statistical Yearbook, about 2400 tons of TMP was produced in China in 2011 [6]. However, only about 40-60% of the given dose can be digested by humans or animals, and the indigested TMP is excreted via faeces or urine into the sewage as its original form [7]. In addition, as less than 10% TMP can be removed by conditional wastewater treatment plants [8, 9], the continuous medical use and incomplete removal have increased its occurrence in the environment. Consequently, bacteria in the environment are exposed to this drug, and

the relatively low concentrations have generated high bacterial resistance toward TMP [10-12]. Recently, TMP has been frequently detected in the effluents of wastewater treatment plants and surface waters at the level of ng L^{-1} to μg L^{-1} [13, 14].

Therefore, removal of TMP from water and wastewater has been a subject of intensive research due to the resistant bacteria can cause disease to humans. Several methods, including photo-Fenton [15], electrochemical oxidation [16], biological processes [17], adsorption by silicates [18], and photocatalytic degradation [19], have been developed for this purpose. Since adsorption onto activated carbon is simple and low-cost operation comparing to other techniques, this technique is regarded as a very effective method to remove undesirable organic contaminants even at very low concentration from aqueous phase [20-22]. Although a few reports are available on adsorption ability of TMP by carbon materials, such as charcoal and commercial activated carbon [23], the underlying mechanism(s) controlling TMP adsorption rate and capacity onto activated carbon are still need to be studied in details.

Generally, activated carbon is composed of short stacks of graphite sheets with well-developed structure and some oxygen containing groups on edges or planes of the graphene structure. As a surface phenomenon, adsorption rate and extent of activated carbon toward a given adsorbate depend on its pore texture and surface chemistry. Activated carbon generally has microporous and/or mesoporous structures and different amounts of acidic and basic groups, which result in different adsorption performance toward TMP. Previous studies have reported that highly microporous activated carbon/charcoal showed high adsorption affinity toward low-sized

adsorbates [24-26]. The presence of oxygen complexes on the surface of carbon material can act as acidic groups and lead to the destabilization of π electrons of graphene structure, eventually altering the electron-donor/-acceptor and acid-base properties of activated carbon. Depending on the multiple groups (three methoxy groups on benzene ring and two amino groups on pyrimidine ring) and the electron-rich aromatic rings in TMP molecule, TMP is expected to react strongly with the corresponding adsorption sites (acidic or basic groups) of activated carbon by chemical interactions, such as ion exchange, Lewis-acid-base interactions, π-π electron donor-acceptor (EDA) interactions and cation-π bonding. However, oxygen containing groups at edges of pores of activated carbon can easily form water clusters with water molecules via hydrogen bond, resulting in blocking entrance of these pores and lowering adsorption capacity [27, 28]. Therefore, the existence of mesopores is also beneficial to the adsorption by providing channels for pollutants diffusing into internal pores. Accordingly, it seems unreasonable to deduce that activated carbon with high microporosity and functional groups content can have large TMP adsorption capacity. Furthermore, although high surface area leads to a large contact area for such interactions and fast adsorption, the entire surface of activated carbon cannot be completely accessible for TMP. Functional groups can also produce attractive and/or repulsive forces to TMP species, causing an enhancement or inhibition of adsorption rate. So far, no relevant study has been conducted to evaluate these effects on the TMP adsorption capacity and rate onto activated carbon.

In order to get a fundamental and systematic understanding of TMP adsorption

onto activated carbon, activated carbon with mainly microporous or mesoporous structures, high or low surface functionalities, and high, low or non- porosities, were prepared to investigate their TMP adsorption performance. The specific mechanisms for TMP adsorption were studied through X-ray photoelectron spectroscopy (XPS) analysis and batch adsorption experiments. By comparing adsorption kinetics and isotherms of TMP, the main physicochemical properties of activated carbon influencing the TMP adsorption rate and capacity were recognized.

2. EXPERIMENTAL SECTION

2.1. Materials.

Trimethoprim (TMP) used was purchased from Shanghai Jingchun biological technology Co., Ltd. (Shanghai). The carbon precursors and activating agents were *Phragmites australis* (biomass), inositol (99%), starch (99%), sodium hydroxide (99.99%), phosphoric acid (85 wt.%), and trimethyl phosphate (98%). Nonporous, pure graphite was purchased from Alfa Aesar and was used as received.

Five different types of activated carbon (AC), namely Micro-AC (micropore AC), Meso-AC (mesopore AC), AC-M (micro-mesopore AC with more surface oxygenated functional groups), AC-L (micro-mesopore AC with less surface oxygenated functional groups) and Non-AC-M (nonporous AC with more surface oxygenated functional groups) were prepared and used in this study. The various process parameters for AC preparation are listed in Table S1 in the Supporting Information. Each kind of activated carbon was prepared by heating the mixture of activating agent

and carbon precursor under an inert atmosphere of nitrogen (150 mL/min). Briefly, carbon precursor was mixed with an activating agent at a certain ratio. Then, the sample was heated at the desired temperature for 1 h. After cooling to room temperature, the carbonized sample was washed with distilled water until the pH of filtrate became steady (~6.0-7.0). Finally, the samples were dried at 105 ^{o}C until the constant weight.

2.2. Characterization.

N_2 adsorption and desorption measurements were performed using a Quadrasorb apparatus (Quantachrome Instruments, USA) at 77 K. Prior to gas adsorption analysis, all samples were degassed at 300 ^{o}C for 6 h. AC samples were analyzed by Raman spectroscopy (Nicolet Almega XR Dispersive Raman, Thermo Electron Corporation, USA) with laser wavelength of 1050 nm. Surface elemental compositions of AC were identified by X-ray photoelectron spectroscopy (XPS). The oxygenated acidic and basic surface groups of AC were measured using the Boehm's titration method.

2.3. Batch Adsorption Experiments.

Batch adsorption experiments were carried out in a thermostated shaker bath (model THZ-82B, Shanghai) at 25 ^{o}C and 120 rmp with 10 mg of adsorbent in 150-mL conical flasks containing 50 mL TMP aqueous solution for 48 h. The pH of each test solution was adjusted to the required value with 0.1 M HCl and NaOH solutions as measured with a pH-meter (PHS-3C, Shanghai). For the kinetics and isotherm experiments, the initial pH of all the solution was chosen to the value of p*K*a

of TMP (7.30), since at this condition the equilibrium pH of each adsorption system was between 7.0-7.5, and these systems contained nearly identical amount of cationic and neutral TMP species. All experiments were conducted in 10 mM NaCl background electrolyte. After equilibrium was reached, samples were filtered and the remaining TMP concentration in filtrate was determined with a spectrophotometer (UV-5100, Shanghai) at 274 nm and a standard curve. The TMP adsorbed onto the adsorbents was calculated by a mass balance. At each condition, adsorption experiments were performed in triplicate and averaged.

3. RESULTS AND DISCUSSION

3.1. Pore Structure and Surface Chemistry.

The specific surface area, pore volume parameters, surface acidic and basic groups, and surface elemental compositions of Micro-AC, Meso-AC, AC-M, AC-L and Non-AC-M are summarized in Table 1. Regarding the surface area of the five different ACs, Micro-AC has the largest specific surface area (~1500 m^2/g), whereas Non-AC-M is almost nonporous with a very small surface area (7.8 m^2/g). Meso-AC has the highest pore volume (1.108 cm^3/g), while AC-M and AC-L have similar pore structure characters. The high porous structures of Micro-AC and Meso-AC and the low/non porous surfaces of AC-M, AC-L and Non-AC-M can also be observed from their SEM images in Figure S1 in Supporting Information. The results of Boehm titration reveal that the ACs are considered acidic (Table 1), which is in agreement with their pH_{pzc} values (< 7.0). The acidic functionalities are determined by

oxygenated groups, such as carboxyl, lactone, and phenolic groups. On the other hand, the basic ones derive mainly from delocalized π-electrons of graphene structures, as well as oxygen groups (chromene, ketone or pyrone). These functional groups can provide effective adsorption sites for TMP removal. For the functional groups, AC-M and Non-AC-M possess the highest content of acidic and basic groups, and Micro-AC and AC-L contain the least.

Table 1. Surface area, pore volume parameters, surface functional groups, and surface elemental composition of the adsorbents.

	Micro-AC	Meso-AC	AC-M	AC-L	Non-AC-M
[a] S_{BET} (m^2/g)	1534	911	393	404	7.8
[b] V_{mic} (cm^3/g)	0.689	0.107	0.108	0.097	0.002
[c] V_{tot} (cm^3/g)	0.778	1.108	0.172	0.171	0.006
V_{mic}/V_{tot} (%)	88.6	9.7	62.8	56.7	33.3
[d] Carboxyl (mmol/g)	0.567	0.831	1.062	0.615	1.124
[d] Lactone (mmol/g)	0.822	0.556	0.835	0.979	0.759
[d] Phenolic (mmol/g)	0.302	0.698	1.269	0.944	1.035
[d] Total acidity (mmol/g)	1.690	2.085	3.165	2.538	2.918
[d] Total basicity (mmol/g)	0.824	1.885	1.910	0.972	1.925
Density of groups (mmol/m^2)	1.64	4.36	12.66	8.69	621
[e] pH_{PZC}	6.22	6.04	6.13	5.75	6.26
[f] C % (atomic percentage)	67.3	63.4	57.9	58.1	54.3
[f] O % (atomic percentage)	32.7	36.6	42.1	41.9	55.7

[a]BET surface area (S_{BET}) was determined by using the Brunauer -Emmett-Teller (BET) theory. [b]Micropore volume was determined by the t-method. [c]Total pore volume was calculated for P/P_0= 0.95. [d]Determined by Boehm's titration [29]. [e]pH_{pzc}: pH at point of zero charge and determined by a batch method [30]. [f]Determined by X-ray photoelectron spectroscopy (XPS).

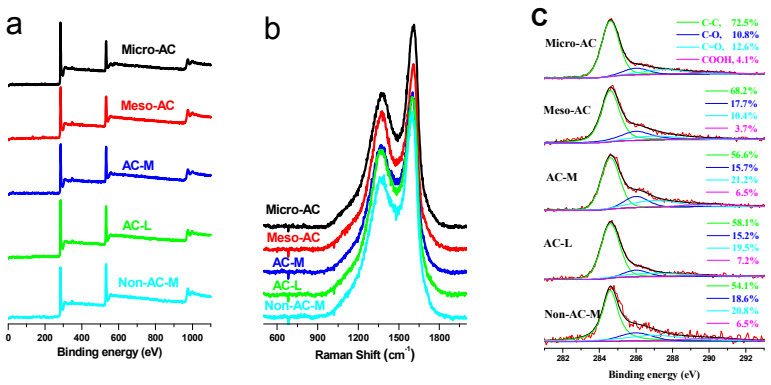

Fig. 1. XPS survey spectra (a) and Raman spectra of the ACs (b). C 1s high-resolution spectra of the ACs (c).

The XPS survey spectra reveal that the functional groups of the ACs are derived from the combination of carbon and/or oxygen elements (Fig. 1a). The ACs show similar Raman spectrum patterns with two broad peaks at around 1350 cm^{-1} for disorder carbon structure (D-band) and 1595 cm^{-1} for graphitic carbon (G-band) (Fig. 1b). The relative intensity ratios of D-band against G-band of the ACs are in the range of 0.6-0.7, indicating they are amorphous carbon materials. These results mean that the chemical interactions between the TMP species and the surfaces of ACs are similar. The C 1S spectra of the AC samples are shown in Fig. 1c. Deconvolution of C 1s spectra exhibites four individual component peaks at: 284.6 eV (graphitic carbon), 286 eV (C-O bond in phenol, alcohol or ether), 287 eV (C=O groups), and 290 eV (carbonyl groups). Fig. 1c also summarize the calculated percentages of graphitic and functional carbon atoms according to the area-simulating curve. The order of %values for functional carbon atoms of the ACs is coincident with their orders of surface O/C ratios.

3.2. Adsorption Isotherms.

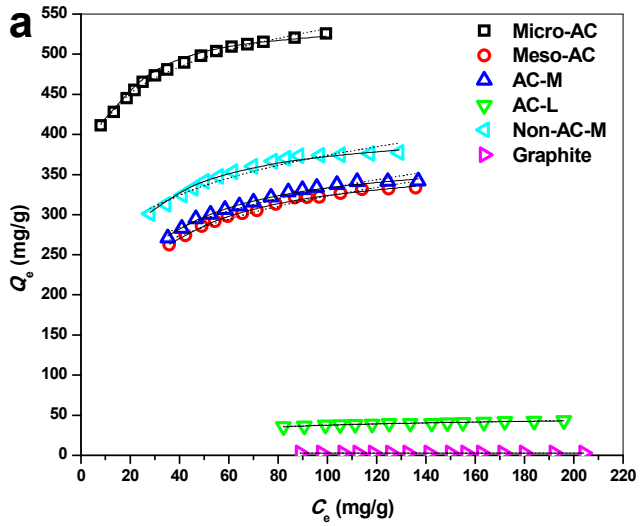

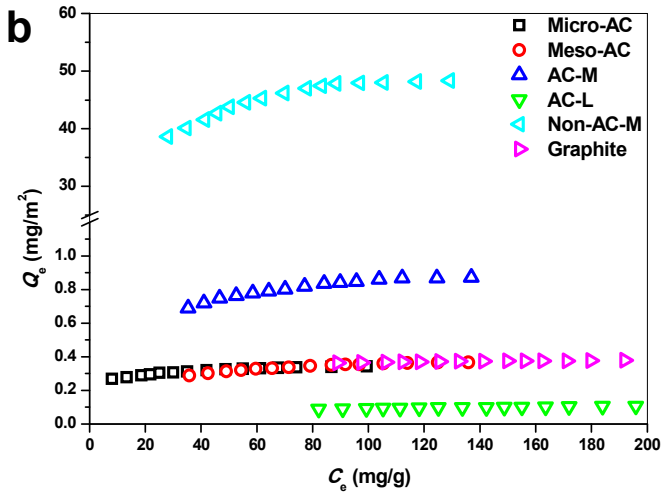

Fig. 2. Adsorption isotherms of TMP for the ACs on unit mass basis (a) and on unit surface area basis (b). The solid and dash lines represent the calculated Langmuir and Freundlich model fitting curves, respectively (dosage = 0.2 g/L, temperature = 25 ± 2 °C, ionic strength = 10 mM NaCl, initial TMP concentrations = 0.3-0.7 mmol/L, and initial pH = 7.30 ± 0.02).

Graphite with 99.9995% graphitized C and surface area of 7.26 m^2/g is also used as adsorbent to evaluate the effect of physic and chemical properties of AC samples on TMP adsorption. Adsorption isotherms of TMP onto the adsorbents are presented in

Fig. 2. The adsorption data were fitted by Langmuir ($Q_e = Q_m K_L C_e/(1 + K_L C_e)$) and Freundlich ($Q_e = K_F C_e^{1/n}$) models, where Q_m (mg/g) is the maximum adsorption capacity according to a complete monolayer adsorption, K_L (L/mg) represents the Langmuir constant, K_F ($mg^{1-n}L^n/g$) is the Freundlich affinity coefficient, and n is the Freundlich linearity index. The fitted parameters are summarized in Table S2 in Supporting Information. As shown in Fig. 2a and Table S2, both the Langmuir and Freundlich models fit the adsorption isotherms very well with $R^2 > 0.95$. However, the Langmuir model seems to fit the equilibrium data better than the Freundlich model with higher R^2 and better representation of the data, which indicates a monolayer adsorption due to the strong interactions between the carbon's surface and TMP species. The very small Freundlich 1/n values (generally not exceeding 0.2) reflect the high adsorption nonlinearity, which can be attributed to the multiple interactions. The maximum adsorption capacity (Q_m, mg/g) of the six adsorbents is in the order of: Micro-AC > Non-AC-M > AC-M ≥ Meso-AC ≫ AC-L ≫ graphite. No apparent linear trends can be observed on the basis of surface area/porosity and surface chemistry, indicating that both chemisorption and physisorption take place simultaneously for TMP adsorption onto the adsorbents. Based on the physicochemical characterizations of AC, three aspects should be considered as follows:

(1) Pore-filling effect. According to the geometry of TMP molecule (7.03*7.5*12.28 A calculated from the software of Chem3D Program), pronounced micropore-filling might invoke TMP adsorption onto porous ACs because the

molecular size of TMP is close to the width of micropores [31]. Thus, even though Micro-AC has the lowest content of surface groups, it exhibits the highest TMP adsorption capacity (Q_m, 543 mg/g) among these carbon samples. As expected, some mesopores (> 2 nm) also contribute to the TMP adsorption by direct pore-filling or enhanced diffusion effect. Meso-AC has slightly higher micropore volume (V_{mic}) and much lower content of surface groups than AC-M, but its TMP adsorption capacity (373 mg/g) is similar to that of AC-M (380 mg/g) since the small-size pores and the functional groups in the internal pores can be accessible for TMP species.

(2) Chemical interactions. Various interactions are expected to exist between TMP species and surface functionalities of AC: 1) π-π EDA interactions; 2) cation-π bonding; 3) Lewis-acid-base interactions; 4) electrostatic attraction; and 5) hydrogen binding. The three methoxy groups (-OCH_3) on benzene ring and two amino groups (-NH_2) on pyrimidine ring are strong electron donating groups, making the aromatic rings π-electron rich. The amino groups can be positively charged at acidic conditions, and are capable of electronic coupling. It is well known that carboxylic and lactonic groups of AC are able to withdraw the electrons of π-electrons on graphene layer, leading to electron deficient π-structures. Therefore, the structures can act as effective π-electron-acceptors to interact strongly with the electron-rich aromatic rings of TMP via the mechanism of π-π EDA interactions. The amino groups of TMP are easily protonated under favorable environmental conditions. The basic groups (Cπ-electrons) can provide adsorption sites of cation-π bonding for the protonated amino group (-NH_3^+) of TMP. The (hydrolyzed) acidic groups can also adsorb the cationic TMP via

electrostatic attraction and Lewis-acid-base interactions. Furthermore, the mechanism of hydrogen bonding also contributes to the adsorption of organic compounds on carbon materials [32]. The $-NH_3$/$-OCH_3$ groups on TMP and the oxygen complexes on the carbon surface can form hydrogen bonds. Accordingly, AC having higher surface oxygen content exhibits higher TMP adsorption through these chemical interactions. As nonporous carbon materials, graphite shows not obvious adsorption, while Non-AC-M exhibits higher TMP adsorption as compared with the other porous activated carbons, except Micro-AC. Similarly, AC-M (393 m^2/g) has a similar Q_m (414 mg/g) to the highly mesoporous activated carbon (Meso-AC, 911 m^2/g, 373 mg/g). The higher content of the surface groups can compensate for the absence of micropore-filling effect and enable stronger adsorption affinity.

(3) Size-exclusion effect. It should be emphasized that size-exclusion effect is expected to exist when TMP is adsorbed onto AC with micropores and surface oxygen complexes. As shown in Fig. 1, some oxygenated groups locate on the external surface of carbon materials. These oxygen groups can adsorb water molecule via hydrogen binding and further form cluster of water molecules. Such phenomenon can prevent TMP species from accessing some adsorption sites of the internal pores. The surface area-normalized adsorption isotherm of the ACs is analyzed and compared as shown in Fig. 2b. The normalized adsorption of TMP follows the order of Non-AC-M $\gg$ AC-M > graphite, Micro-AC, Meso-AC > AC-L. The surface area-normalized adsorption on Non-AC-M is significantly higher than that on the other carbons by approximately 50-500 times in the tested concentration range, mainly because of its

highest density of functional groups on unit surface area basis and the absence of size-exclusion effect. As another nonporous carbon material, graphite with free-oxygen surface is also not expected to invoke the pore effect (micropore-filling or size exclusion). It shows similar normalized adsorption of TMP as Micro-AC and Meso-AC. Similarly, the normalized adsorption capacities of Micro-AC and Meso-AC are identical and approximately 2.5 time less than that of AC-M. Their low normalized adsorption are mainly due to that a large part of pores with pore width less or much larger than the size of TMP are useless for TMP adsorption. The size-exclusion effect is most obvious for TMP adsorption on AC-L. AC-L has similar pore characteristics to AC-M, and its density of functional groups is about 30% less than that of AC-M. However, the normalized TMP adsorption of AC-L is about 8 times less than that of AC-M. As compared with AC-M, AC-L contains much more oxygen complexes on the edges of pores (see XPS analysis, Fig. 1), thus the adsorption sites in the pores are difficult for TMP to access. Similarly, although AC-M has some micropores and slightly higher functional groups than Non-AC-M, it exhibits moderately lower TMP adsorption. The relatively high TMP adsorption for Non-AC-M can be explained by its accessible surface and high content of surface groups. Accordingly, the oxygen complexes around pore entrances restrict TMP admittance, and result in the markedly size-exclusion effect and the low TMP adsorption.

The results of adsorption isotherms for the ACs indicate that (1) micropore-filling effect leads to the high adsorption affinity of low molecular-sized TMP onto highly

microporous AC; (2) the presence of mesopores allows TMP entering the internal pores, and guaranteeing TMP adsorption on these adsorption sites effectively; (3) strong interactions exist between TMP species and the surface groups of AC, and (4) the existence of large amount of oxygen containing groups on the edges of narrow pores of AC inhibits TMP uptake profoundly by limiting TMP transport into the internal pores.

3.3. Adsorption Kinetics.

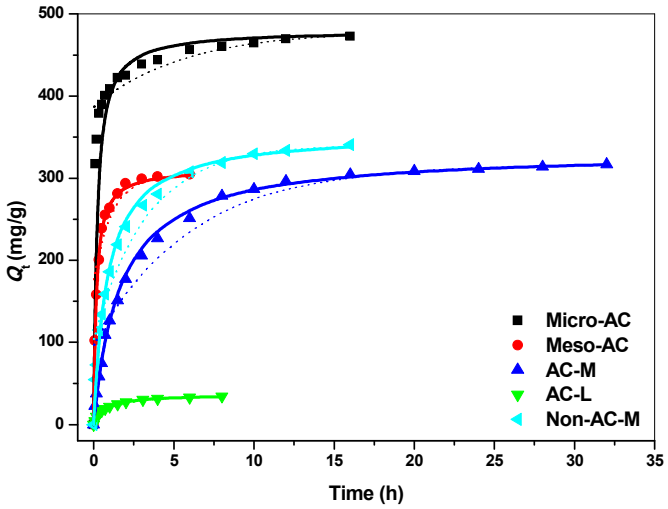

Fig. 3. Kinetics of TMP adsorption onto the ACs. The dash and solid lines represent the calculated pseudo-first and pseudo-second order model fitting curves, respectively (dosage = 0.2 g/L, temperature = 25 ± 2 ^{o}C, ionic strength = 10 mM NaCl, initial TMP concentration = 0.4 mmol/L (116 mg/L), and initial pH = 7.30 ± 0.02).

Since adsorption rate is an important factor for practical operation, adsorption kinetics of TMP for the five ACs was investigated. The effect of contact time on TMP adsorption is presented in Fig. 3. The TMP adsorption increases rapidly, then rises gradually and reaches equilibrium within 35 h for all samples tested. As expected, the

five ACs exhibit completely different adsorption rates and equilibrium times. To quantitatively compare the TMP adsorption rates on the ACs, the pseudo-first order and pseudo-second order models were used to fit the experimental data, and the kinetic parameters are shown in Table S3 in Supporting Information. According to Fig. 3 and Table S3, the pseudo-second order model fits all the experimental data better than the pseudo-first order model, which implies that chemical interactions are involved in TMP adsorption. The calculated rate constants of the ACs follows an order of Micro-AC > Meso-AC > Non-AC-M > AC-M ≫ AC-L, which does not correlate with neither porosity nor surface functionalities. These results demonstrate that TMP adsorption rate on the carbon materials is controlled by both pore diffusions and chemical interactions.

It can also be seen from Fig. 3 that the initial TMP adsorption for Micro-AC and Meso-AC is much faster than that for AC-M, AC-L and Non-AC-M. For example, approximately 80% of adsorption is achieved within 1 h for Micro-AC and Meso-AC, while only 20-50% adsorption is accomplished for AC-M, AC-L and Non-AC-M. Particularly, Non-AC-M shows relatively slow adsorption and long equilibrium time. These results strongly support that chemical adsorption for TMP removal is a much slower process as compared to pore-filling one. Previous studies have explored the micropore-filling mechanism to explain the enhanced adsorption rates of organic chemicals to microporous adsorbents [33, 34]. However, as adsorption increases, the internal pores will be hard to access for TMP due to the pore-width decrease by the accumulation of TMP adsorption. Thus, the presence of mesopores is beneficial for

adsorbate to diffuse into the internal pores. Accordingly, although the equilibrium adsorption capacity of Micro-AC (479 mg/g) is much larger than that of Meso-AC (304 mg/g), its equilibrium time (within 16 h) is longer than that of Meso-AC (within 6 h) (see Fig. 3). The longer adsorption equilibrium time required by Micro-AC indicates that diffusion of TMP within micropores also controls the adsorption rate of AC with microporosity. This result can also be confirmed from observation that the nonporous Non-AC-M shows a similar amount of surface functional groups as AC-M, but has shorter equilibrium time. Meanwhile, the oxygen-containing groups on the edges of pores further inhibit the diffusion of TMP molecules into the pores due to steric effect, which is most obvious for TMP adsorption onto AC-L as evidenced by its dramatically low adsorption among all the ACs.

According to the results discussed above, we can draw some conclusions about the effects of pore texture and surface functional groups on TMP adsorption rate as follows: (1) both diffusion of TMP in micropores and chemical interactions between TMP species and surface functional groups are slow processes; (2) the presence of mesopores can promote the diffusion of TMP into internal pore and improve adsorption rate; and (3) the oxygen complexes represented on edges of the pores can obviously restrain TMP diffusion into narrow pores.

3.4. Effect of Solution pH on Adsorption.

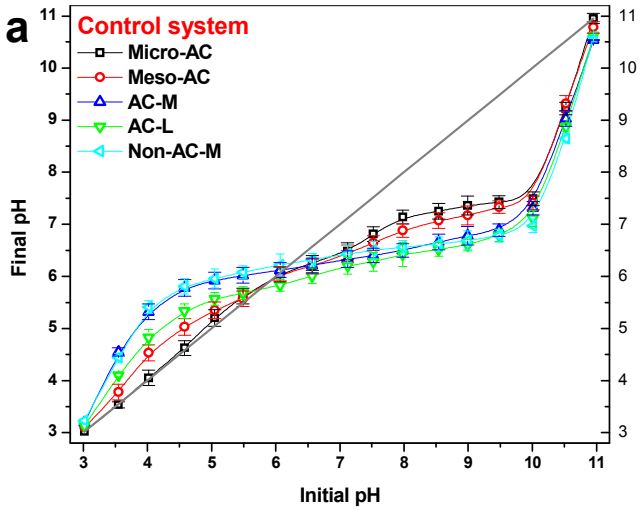

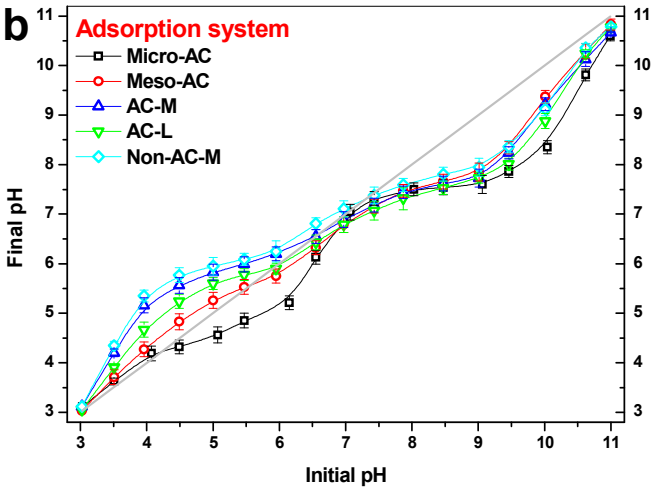

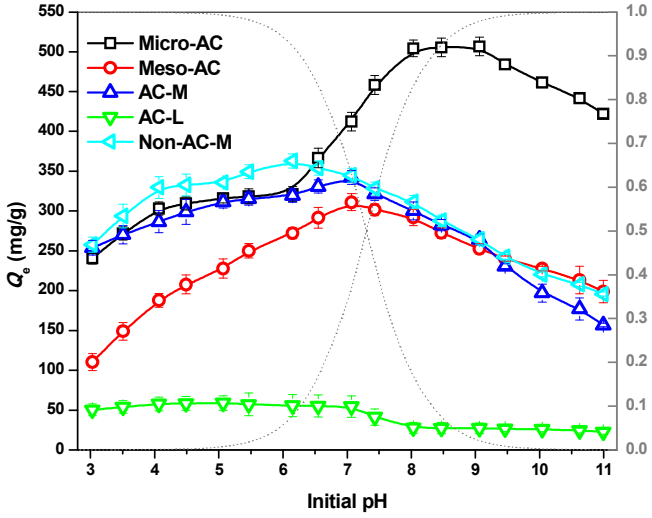

Fig. 4. Variations of solution pH before and after equilibrium: control system and adsorption system are the batch experiments by adding carbon samples to distilled water (a) or TMP solution (b) with different initial pH. Effect of pH on the adsorption of TMP onto the ACs (c) (dosage = 0.2 g/L, temperature = 25 ± 2 ^{o}C, ionic strength = 10 mM NaCl, and initial TMP concentration = 0.4 mmol/L).

As above-mentioned, TMP adsorption onto the ACs involves strong interactions between TMP species and the surface groups. The speciation of TMP and surface charge properties of AC are susceptible to solution pH, because the two amino groups of TMP molecule can be protonated by excess H^+ ions in bulk solution, and the acidic and basic groups of AC can also be deprotonated or protonated. Thus, solution pH can be favorable or unfavorable to adsorption. To recognize these interactions for TMP adsorption, the effects of pH on adsorption were evaluated with pH ranging from 3.0 to 11.0 and are represented in Fig. 4.

Fig. 4a and b illustrate the equilibrium pH levels of control and adsorption samples. Obviously, Micro-AC and Meso-AC have less acidic and basic groups, thereby exhibiting the lowest acid/base neutralization capacity (Fig. 4a). By

comparing the equilibrium pH levels of all samples at acidic condition, the final pH values of control samples are higher than those of adsorption samples, which indicates that adsorption of TMP is accompanied by releasing H^+ ions into the bulk solution, namely a proton exchange mechanism. For instance, the final pH levels for Micro-AC adsorption samples are lower than their initial pH levels after TMP adsorption. The proton exchange mainly derives from the cation-π interactions between protonated Cπ electrons and $-NH_3^+$ of TMP as well as acid-base reactions of acidic groups and $-NH_3^+$ of TMP.

Previous studies have well demonstrated the formation of cation-π bonding between protonated amino group and (protonated) Cπ-electrons [35, 36]. The Cπ electrons within graphene structures and amino groups (pK_a of 7.30) of TMP are easily protonated under acidic conditions [37]. When initial pH increases from 2 to 11, the charge of activated carbon surface will be converted from positive to negative electricity, and the cationic TMP will turn into neutral TMP molecule. Therefore, it means that the electrostatic repulsion exists and impedes TMP adsorption at low pH conditions. Additionally, when the amino groups are deprotonated, the electron giving ability will decrease dramatically, and the π-π EDA interactions will be weakened. However, the ACs show an obvious decrease in TMP adsorption at initial pH between 7.0 and 11.0 and a higher TMP adsorption under acidic conditions in comparison with that under basic conditions (AC-M, AC-L and Non-AC-M) (see Fig. 4c). These results reflect that the existence of cation-π interactions promotes the adsorption cationic TMP species. In addition, Lewis-acid-base interactions between amino groups of

TMP and carboxylic and phenolic hydroxy groups have been reported in previous studies about adsorption of organic compounds to AC [38, 39]. Thus, it can be deduce that the reaction between $-NH_3^+$ groups and the acidic groups (especially carboxylic groups) is another contributor to lower final pH of adsorption samples, which is demonstrated by XPS analysis (Fig. 5). Lewis-acid-base interactions can also be observed from the higher final pH levels for the adsorption samples compared to those for the control samples at high initial pH (above 7) (Fig. 4b), as less acidic groups is left for neutralizing excess OH^- ions in solution. The XPS survey and N 1s spectra of Non-AC-M before and after TMP adsorption at different initial pH (3.0, 7.3 and 11.0) are shown in Fig. 5. One peak appears at 400 eV for the XPS survey spectra of TMP-adsorbed Non-AC-M samples, indicating the fixation of TMP onto the ACs (Fig. 5a). It is also shown in Fig. 5b, c and d that the peak area of N 1s on TMP-adsorbed Non-AC-M surfaces follows the order of TMP-Non-AC-M-7.3 > TMP-Non-AC-M-3.0 > TMP-Non-AC-M-11.0, which is consistent with the TMP adsorption capacity of Non-AC-M at corresponding pH of the solution. The N 1s spectra of the samples comprise two peaks, which are assigned to the nitrogen atoms in the forms of -CO-NH- (399.6 eV) and $C-NH_2$ (400.4 eV). The results elucidates that reaction occurs between amine functional groups on TMP and carbonyl functional groups on activated carbon.

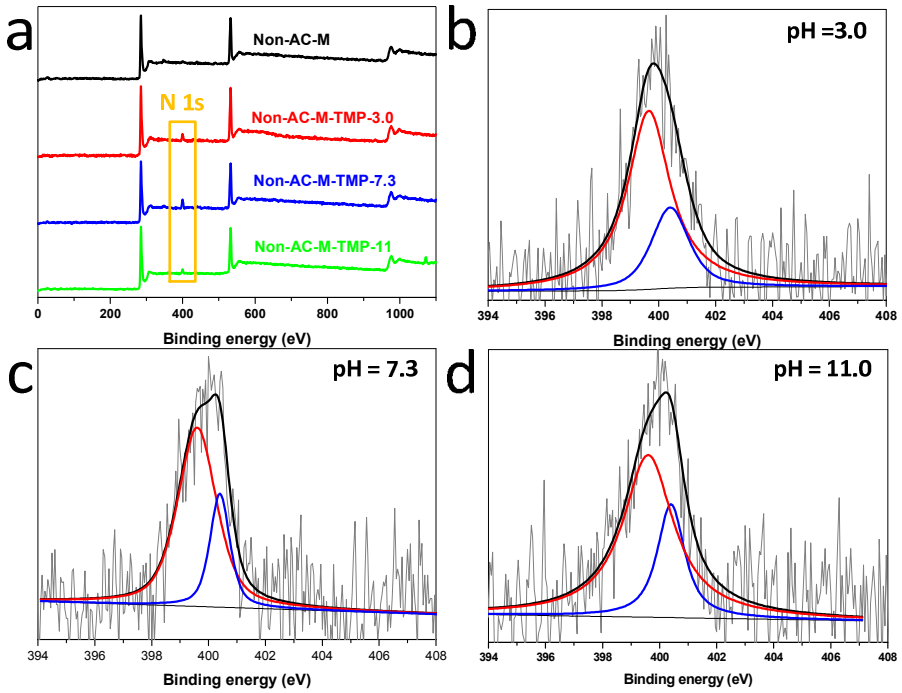

Fig. 5. XPS survey spectra and N 1s spectra of Non-AC-M before and after TMP adsorption at initial solution pH of 3.0, 7.3 and 11.0.

All ACs used in this study are dominated by the graphitized carbons with some associated oxygen complexes, and thus they present the same types of adsorptive interactions with TMP species. However, they exhibit different variable trends (Fig. 5c). The results are mainly related to the difference in amounts of acidic and basic groups of the ACs. These groups can neutralize the excess H^+ and OH^- ions in bulk solution (see Fig. 5a), and affect the species of TMP, eventually resulting in the different adsorption patterns. As shown in Fig. 5c, the TMP adsorption capacities of the ACs increase with increasing pH, and then decrease with pH. The low TMP adsorption at low pH is attributed to electrostatic repulsion as well as the competition from excess H^+ ions in the solution. Moreover, the less available cationic TMP leads to the free of cation-π interactions, decreasing the TMP adsorption at high pH. Since

TMP is dominated by the cationic form and the ACs surface is negatively charged at moderate initial pH levels (~6-9), the enhanced electrostatic attraction and the existence of cation-π interactions promote the TMP adsorption.

It should be emphasized that in acidic pH range Micro-AC and Meso-AC show the highest increase in TMP adsorption, which is due to their lowest content of surface basic groups. In particular, the adsorption to Micro-AC is even lower than that of AC-M at initial pH 2-6.5. The pore-filling is proposed to be an important mechanism participating in the TMP adsorption to Micro-AC and Meso-AC. At acidic conditions, the surfaces of the ACs are positively charged, and cannot be easily accessible for cationic TMP molecules, thereby resulting in the low adsorption. However, AC-M and Non-AC-M have high content of acidic and basic groups, which can buffer the excess H^+ and reduce changes of their surface net charges. Thus, they can have a relatively steady TMP at acidic conditions.

4. CONCLUSION

Five types of activated carbons with different porosities and functional groups contents (mainly microporous or mesoporous structures, high or low surface functionalities, and high, low or non- porosities) were prepared and used as adsorbents for TMP removal. The underlying mechanisms controlling TMP adsorption rate and capacity onto activated carbons are expatiated in this study. The diffusion of TMP in micropores and reactions between TMP species and functional groups are slow processes, and the mesopores promote the diffusion of TMP into the

internal pores and adsorption rates. The micropore-filling mechanism accounts for the high adsorption affinity of low molecular-sized TMP species to a highly microporous activated carbon compared to the mesoporous and low porous activated carbons. Surface functional groups give significant contribution toward TMP adsorption capacity, primarily through providing strong chemical interactions, such as Lewis-acid-base interactions, π-π EDA interactions, electrostatic attraction/repulsion, cation-π bonding, and hydrogen binding. However, the oxygen-containing groups block the micropore entrances and reduce the TMP adsorption. The high content of acidic and basic functional groups neutralizes the excessive base and acid in the bulk solution and keeps the high TMP adsorption in a large solution pH.

Acknowledgements

This work was supported by the Independent Innovation Foundation of Shandong University (2012JC029), Natural Science Foundation for Distinguished Young Scholars of Shandong Province (JQ201216) and National Water Special Project (2012ZX07203-004). The authors gratefully acknowledge the fund from Shanghai Tongji Gao Tingyao Environmental Science and Technology Development Foundation.

References

1. N. Datta and R. W. Hedges, *J. Gen. Microbiol.*, 1972, **72**, 349-355.

2. K. B. Barnes, J. Steward, J. E. Thwaite, M. S. Lever, C. H. Davies, S. J.

Armstrong, T. R. Laws, N. Roughley, S. V. Harding, T. P. Atkins, A. J. H. Simpson and H. S. Atkins, *Int. J. Antimicrob. Ag.*, 2013, **41**, 552-557.

3. S. Z. Wiktor, M. Sassan-Morokro, A. D. Grant, L. Abouya, J. M. Karon, C. Maurice, G. Djomand, A. Ackah, K. Domoua, A. Kadio, A. Yapi, P. Combe, O. Tossou, T. H. Roels, E. M. Lackritz, D. Coulibaly, K. M. D. Cock, I.-M. Coulibaly and A. E. Greenberg, *The Lancet*, 1999, **353**, 1469-1475.

4. X. Anglaret, G. Chêne, A. Attia, S. Toure, S. Lafont, P. Combe, K. Manlan, T. N'Dri-Yoman and R. Salamon, *The Lancet*, 1999, **353**, 1463-1468.

5. J. Kuang, J. Huang, B. Wang, Q. Cao, S. Deng and G. Yu, *Water Res.*, 2013, **47**, 2863-2872.

6. Chinese Medical Statistical Yearbook, Beijing, 2011, 71.

7. J. Siemens, G. Huschek, C. Siebe and M. Kaupenjohann, *Water Res.*, 2008, **42**, 2124-2134.

8. R. H. Lindberg, U. Olofsson, P. Rendahl, M. I. Johansson, M. Tysklind and B. A. V. Andersson, *Environ. Sci. Technol.*, 2005, **40**, 1042-1048.

9. X. Luo, Z. Zheng, J. Greaves, W. J. Cooper and W. Song, *Water Res.*, 2012, **46**, 1327-1336.

10. B. E. Murray, E. R. Rensimer and H. L. DuPont, *New Engl. J. Medi.*, 1982, **306**, 130-135.

11. D. T. Steinke, R. A. Seaton, G. Phillips, T. M. MacDonald and P. G. Davey, *J. Antimicrob. Chemoth.*, 1999, **43**, 841-843.

12. D. Bastien, M. C. C. J. C. Ebert, D. Forge, J. Toulouse, N. Kadnikova, F.

Perron, A. Mayence, T. L. Huang, J. J. Vanden Eynde and J. N. Pelletier, *J. Med. Chem.*, 2012, **55**, 3182-3192.

13. A. J. Watkinson, E. J. Murby, D. W. Kolpin and S. D. Costanzo, *Sci. Total Environ.*, 2009, **407**, 2711-2723.

14. B. Li and T. Zhang, *Chemosphere*, 2011, **83**, 1284-1289.

15. I. N. Dias, B. S. Souza, J. H. O. S. Pereira, F. C. Moreira, M. Dezotti, R. A. R. Boaventura and V. J. P. Vilar, *Chem. Eng. J.*, 2014, **247**, 302-313.

16. T. González, J. R. Domínguez, P. Palo, J. Sánchez-Martín and E. M. Cuerda-Correa, *Desalination*, 2011, **280**, 197-202.

17. A. L. Batt, S. Kim and D. S. Aga, *Environ. Sci. Technol.*, 2006, **40**, 7367-7373.

18. D. Zadaka, Y. G. Mishael, T. Polubesova, C. Serban and S. Nir, *Appl. Clay Sci.*, 2007, **36**, 174-181.

19. S. Sarkar, R. Das, H. Choi and C. Bhattacharjee, *RSC Adv.*, 2014, **4**, 57250-57266.

20. J. M. Salman, V. O. Njoku and B. H. Hameed, *Chem. Eng. J.*, 2011, **173**, 361-368.

21. H. L. Parker, A. J. Hunt, V. L. Budarin, P. S. Shuttleworth, K. L. Miller and J. H. Clark, *RSC Adv.*, 2012, **2**, 8992-8997.

22. A. S. Bhatt, P. L. Sakaria, M. Vasudevan, R. R. Pawar, N. Sudheesh, H. C. Bajaj and H. M. Mody, *RSC Adv.*, 2012, **2**, 8663-8671.

23. S. H. Kim, H. K. Shon and H. H. Ngo, *J. Ind. Eng. Chem.*, 2010, **16**, 344-349.

24. K. Y. Foo and B. H. Hameed, *Chem. Eng. J.*, 2011, **173**, 385-390.

25. K. Y. Foo and B. H. Hameed, *Chem. Eng. J.*, 2012, **187**, 53-62.

26. Y. Sun, C. Chen, D. Shao, J. Li, X. Tan, G. Zhao, S. Yang and X. Wang, *RSC Adv.*, 2012, **2**, 10359-10364.

27. Z. Zhou, Z. Zhang, H. Peng, Y. Qin, G. Li and K. Chen, *RSC Adv.*, 2014, **4**, 5524-5530.

28. K. Wang, H. Wang, S. Ji, H. Feng, V. Linkov and R. Wang, *RSC Adv.*, 2013, **3**, 12039-12042.

29. H. P. Boehm, *Carbon*, 2002, **40**, 145-149.

30. J. J. M. Órfão, A. I. M. Silva, J. C. V. Pereira, S. A. Barata, I. M. Fonseca, P. C. C. Faria and M. F. R. Pereira, *J. Colloid Interf. Sci.*, 2006, **296**, 480-489.

31. S. Ismadji and S. K. Bhatia, *Langmuir*, 2001, **17**, 1488-1498.

32. D. Lin and B. Xing, *Environ. Sci. Technol.*, 2008, **42**, 7254-7259.

33. P. Pendleton and A. C. Zettlemoyer, *J. Colloid Interf. Sci.*, 1984, **98**, 439-446.

34. C. Moreno-Castilla, *Carbon*, 2004, **42**, 83-94.

35. M. Keiluweit and M. Kleber, *Environ. Sci. Technol.*, 2009, **43**, 3421-3429.

36. D. A. Dougherty, *Accounts Chem. Res.*, 2012, **46**, 885-893.

37. J.-W. Shim, S.-J. Park and S.-K. Ryu, *Carbon*, 2001, **39**, 1635-1642.

38. W. Chen, L. Duan, L. Wang and D. Zhu, *Environ. Sci. Technol.*, 2008, **42**, 6862-6868.

39. E. K. Putra, R. Pranowo, J. Sunarso, N. Indraswati and S. Ismadji, *Water Res.*, 2009, **43**, 2419-2430.

Table captions:

Table 1. Surface area, pore volume parameters, surface functional groups, and surface elemental composition of the adsorbents.

Figure captions:

Fig. 1. XPS survey spectra and Raman spectra of the ACs.

Fig. 2. Kinetics of TMP adsorption onto the ACs.

Fig. 3. Adsorption isotherms of TMP for the ACs (a) on unit mass basis and (b) on unit surface area basis.

Fig. 4. Variations of solution pH before and after equilibrium: control system and adsorption system are the batch experiments by adding carbon samples to distilled water (a) or TMP solution (b) with different initial pH. Effect of pH on the adsorption of TMP onto the ACs (c).

Fig. 5. XPS survey spectra and N 1s spectra of Non-AC-M before and after TMP adsorption at initial solution pH of 3.0, 7.3 and 11.0.